Nanoscience and Nanometrology
2022; 8(1): 1-9
http://www.sciencepublishinggroup.com/j/nsnm
doi: 10.11648/j.nsnm.20220801.11
ISSN: 2472-3622 (Print); ISSN: 2472-3630 (Online)

Structural and Optical Properties of Er^{3+} Doped Tellurite Glass with Copper Oxide Nanoparticles Embedment

Zahra Ashur Said Mahraz[1, 2, *], Nur Ezzati Nabilah Syaqilah Abdul Hamid[1], Ezza Syuhada Sazali[1, *], Faizani Mohd Noor[1], Md. Rahim Sahar[1], Syariffah Nurathirah Syed Yaacob[1], Aizul Nahar Harun[1]

[1]Faculty of Science, Universiti Teknologi Malaysia, Skudai, Malaysia

[2]College of Education-Zulten, University of Sabratha, Zulten, Libya

Email address:

mabutm.mabutm@yahoo.com (Z. A. S. Mahraz)

[*]Corresponding author

To cite this article:

Zahra Ashur Said Mahraz, Nur Ezzati Nabilah Syaqilah Abdul Hamid, Ezza Syuhada Sazali, Faizani Mohd Noor, Md. Rahim Sahar, Syariffah Nurathirah Syed Yaacob, Aizul Nahar Harun. Structural and Optical Properties of Er^{3+} Doped Tellurite Glass with Copper Oxide Nanoparticles Embedment. *Nanoscience and Nanometrology*. Vol. 8, No. 1, 2022, pp. 1-9. doi: 10.11648/j.nsnm.20220801.11

Received: November 4, 2021; **Accepted**: December 1, 2021; **Published**: April 20, 2022

Abstract: Improving the optical properties of copper oxide nanoparticles (CuO NPs) in tellurite glass is crucial for the development of efficient solid state laser. In this work, we report the results of structurally-induced transitions in melt-quench synthesized CuO NPs integrated Er_2O_3 doped multicomponent tellurite glasses. Based on the predecessors' work, we optimized the components of such glasses to observe its effects on the structural, physical and optical properties of the glasses were characterized using density, XRD, HTEM, FTIR, UV–vis-IR absorption and PL spectroscopy. The variations of physical properties are measured and the hardness of the glasses is performed by using Vickers Microhardness. XRD analysis confirmed the amorphous nature of the prepared glass sample. The presence of CuO NPs is verified by using HRTEM with lattice spacing 0.23 nm at (111) plane orientation inside the glass matrix. FTIR spectrum shows that the glasses are made up of $[TeO_4]$ and $[TeO_3]$ structural units. Absorption spectra of glasses consisted of seven significant bands from the ground sate $^4I_{15/2}$ to the excited states $^4F_{7/2}$, $^2H_{11/2}$, $^4S_{3/2}$, $^4F_{9/2}$, $^4I_{9/2}$, $^4I_{11/2}$ and $^4I_{13/2}$ are attributed to excited states around 488, 522, 545, 652, 799, 973 and 1530 nm, wherein $^4I_{15/2}$ to $^4I_{9/2}$ transition in Er^{3+} disclosed the highest intensity. The decrease in bonding parameter increases the formation of more covalent bond in the glass network. Appreciable changes have been observed in the photoluminescence emission intensity with the change in Cu NPs concentration in the medium. Down-conversion emission spectra under 380 nm excitation shows four peaks centered at 408, 530, 550, and 660 nm. Meanwhile, up-conversion emission spectra under excitation 980 nm shows three peaks centered at 530, 550, and 660 nm. The enhancement in the luminescence is attributed to the localized electric field in vicinity of nanoparticles, while, the quenching effect is responsible from the large formation of multipoles interaction that leads to the energy transfer from RE ions to NPs. Intense green emission obtained from the proposed glasses could be a potential gain medium for solid-state laser medium.

Keywords: Tellurite Glass, CuO NPs, FTIR, Absorption, Emission

1. Introduction

The use of tellurite glasses as a host material is demanded due to their distinct optical properties compare to other oxide glasses. It has high linear and non-linear refractive indices, high gain density, low glass transition, wide transparency window, low phonon energy environment to minimize the non-radiative losses, good thermal stability and high chemical durability [1]. Moreover, tellurite glass has Te-O bond that can break easily which make them a promising host for the heavy metal or rare earth ions (REIs) [2]. The latter feature is critical for RE-doped glasses when it comes to application point of view, where it is absolutely essential to achieve population inversion in lasers or up-conversion

emissions. These types of inorganic oxide glasses are suitable for wide range of applications including the solid state lasers, sensing devices, light emitting diodes (LED), fibre optics and so on [1-3].

Because of the rich electronic shell structure, the RE dopants can yield significant emissions in the visible and near-infrared spectral regions which contributes to easy pumping, tunable dye laser. Therefore, these glasses are usually called as activated glasses where they are capable of emitting radiation (luminescence) after being excited, which is responsible for the emission wavebands [4]. Hence, REIs will have capability of coloring glass through absorptive transitions together with a set of states capable of emitting light. Tellurite glasses doped REIs such as Nd^{3+}, Sm^{3+} [5, 6], Yb^{3+}, Eu^{3+}, Tb^{3+}, and Pr^{3+} [7-9] ions are also investigated for their lasing action in the visible and near infrared regions and their superior optical and structural properties are manifested. Amongst various REIs, Er^{3+} ion is one of the interesting candidates because it has well separated energy states, broad range of emission characteristics and emits intense green and red light. Although the optical response of REIs in tellurite glasses are comparably better than many of other glassy candidates, the emission intensity and quantum efficiency of these materials yet to be improve [7].

In recent years, modifications on RE-doped tellurite glass system by combining with transition metal ions have attracted great attention owing to their properties that leads toward worldwide applications [3]. Transition metal ions serve as structural probes for the environment of the dopant for glass, since they are characterized by partially filled *d*-shell and are strongly related with the magnetic, electrical and optical features of glasses [10]. With the addition of nanoparticles (both silver and gold NPs) [11-14] the up-conversion emissions of E^{3+} doped tellurite glasses could be improved, although some reports on the quenching of up-conversion luminescence by metal NPs could be found [15, 16]. The origin of the observed enhancements is somehow controversial as it sometimes attributed to (i) an energy transfer (ET) process from metal species to RE ions [17], (ii) a local field enhancement around the rare earth ions due to presence of metallic NPs (iii) NPs removes the OH radical groups and results in better quantum efficiency of RE ions [18]. Recently, transition metal oxide such as copper oxide (CuO) are of considerable interest due to its behavior that can exist in two valence states in the glass system; the monovalent Cu^{1+} ($3d^{10}$) and the divalent state Cu^{2+} ($3d^{9}$) where Cu^{2+} ions present as the stable element [19]. Addition of CuO NPs into the glass network makes the glass electrically good semiconductor and super-paramagnetic [9]. CuO NPs attracts huge attention due to its remarkable cost effective compare to silver and gold NPs as well as superior electrical/thermal conductivity than other noble metals [20]. CuO NPs doped glasses have sparked interest in the field of materials science due to their enormous potential for various applications such as lighting systems, optical fibres and photonic waveguides [21]. Therefore, a better understanding of the luminescence behavior of Er^{3+} ions in vicinity of CuO NPs is essential especially considering their importance for the real time applications. Driven by this idea, we aimed to study the effect of CuO NPs on physical, structural and optical properties of Er^{3+} doped tellurite glasses. The up-conversion (UC), down-convesion (DC) and nearinfrared emissions were collected and variation of the spectral intensity by addition of the CuO NPs were studied and discussed associated with the energy transfer mechanism of such glasses.

2. Experimental Methods

The glass composition of (69–x)TeO_2–10ZnO–10MgO–10Na_2O–1Er_2O_3–(y)CuO (where x = 0.05, 0.10, 0.25, 0.50, 1.00 and 1.50 mol%) are synthesized using melt quenching technique in several batches of 15g. The required composition consist of high quality of raw materials (as listed in Table 1) were mixed for 30 minutes to produce homogenous mixture and the mixtures were melted in a crucible at 900°C for 30 minutes into the furnace. Throughout the process, the melt were stirred frequently. Then, the melt was poured very fast on a metal plate in another furnace and annealed for 3 hours at 300°C in order to prevent crystallization and eliminate internal stress. The sample was left until the temperature decreased slowly to room temperature. Finally, the samples were cut and polished for the characterizations process.

The hardness of the materials was performed using HMV-2 series Shimadzu Micro Hardness Tester. The load is set to 980.7 m Newton and applied slowly by pressing the indenter at 90° into the sample surface. Perkin Elmer FTIR spectrometer was used to determine chemical identification of the sample in the range of 400 to 4000 cm^{-1}. The absorption spectra were recorded using Shimadzu UV-3600 Plus UV-Vis-NIR spectrophotometer meanwhile the emission spectra were recorded from 300–700 nm wavelengths using Horiba FluoroMax-4 Photoluminescence spectrophotometer. Archimedes principle is used to measure the density of the glass by using Prescisa Balance XT 220A. Distilled water is used as the immersion liquid. The density measurement of the glass given by,

$$\rho = \frac{W_a}{W_a - W_l}(\rho_l - \rho_a) + \rho_a \quad (1)$$

where W_a refers to the weight of the sample in air whereas, W_l signifies weight in immersion liquid and the density of the immersion fluid (distilled water = 1 $g\,cm^{-3}$) and density of air (0.001 $g\,cm^{-3}$) represent by ρ_l and ρ_a.

The value of density from above equation is necessary to determine the molar volume V_m by using stated equation as below,

$$V_m = \frac{M}{\rho} \quad (2)$$

where M refers to the molecular weight of the sample calculated to determine the composition of the glass. The ionic packaging density is calculated by,

$$V_t = \left(\frac{1}{V_m}\right)\sum\left(V_i x_i\right) \quad (3)$$

Where V_i is packing density parameter (m^3/mol) and x_i is molar fraction (mol%). V_i can be calculate using the following equation,

$$V_i = \left(\frac{4\pi N_A}{3}\right)\left[Xr_M^3 + Yr_O^3\right] \quad (4)$$

Where N_A, r_M and r_o refer to Avogadro's number (mol^{-1}), ionic radius of metal and ionic radius of oxygen respectively.

The refractive index of the glass samples are calculated by,

$$\frac{n^2-1}{n^2+2} = 1 - \sqrt{\frac{E_g}{20}} \quad (5)$$

where E_g is the glass optical band gap. Furthermore Molar refractivity R_M can be defined as,

$$\frac{n^2-1}{n^2+2}\,(V_M) = R_M \quad (6)$$

The polarizability of the glass, α_e can be calculated by,

$$R_M = \frac{4}{3}\,\pi N_A \alpha_e \quad (7)$$

where N_A is the Avogadro's number. The following expression is suggested by Mott and Davis to determine the optical band gap energy, E_g,

$$\alpha\,(v) = B\,(hv - E_g)^n / hv \quad (8)$$

where B is a constant, n = ½ for direct transition, n = 2 for indirect transition. In many crystalline and non-crystalline semiconductors, the $\alpha(v)$ exponentially dependence on hv. This exponentially dependence known as Urbach rule given by,

$$\alpha\,(v) = B\exp\left(\frac{hv}{E_u}\right) \quad (9)$$

where E_u is Urbach energy. The absorption spectra used to determine the nephelauxetic ratio (β) and bonding parameter (δ) given by,

$$\beta = \frac{v_c}{v_a} \quad (10)$$

where v_c is the wavenumber (cm^{-1}) of specific transitions in host matrix and v_a is a corresponding wavenumber (cm^{-1}) of the same transitions in aqua ion system. Nephelauxetic effect indicates the expansion of electron cloud due to the expanse of nearly filled shell because of transfer of ligands towards the core of central RE ions [22]. The bonding parameter can be expressed using the following formula,

$$\delta = \frac{1-\bar{\beta}}{\bar{\beta}} \quad (11)$$

where $\bar{\beta}$ is average value for specific transitions. The field environment of the host network determines the bonding parameter of the glass [23].

Table 1. *Nominal compositions of the studied glasses.*

Glass	Composition (mol%)					
	TeO_2	ZnO	MgO	Na_2O	Er_2O_3	CuO
S1	68.95	10.0	10.0	10.0	1.0	0.05
S2	68.90	10.0	10.0	10.0	1.0	0.10
S3	68.75	10.0	10.0	10.0	1.0	0.25
S4	68.50	10.0	10.0	10.0	1.0	0.50
S5	68.00	10.0	10.0	10.0	1.0	1.00
S6	67.50	10.0	10.0	10.0	1.0	1.50

3. Results and Discussions

3.1. Density, Molar Volume and Ionic Packaging Density

Measured values of all the physical parameters of the synthesized glass samples are tabulated in Table 2. As the ions and ionic group are tightly packed together in the glass structure, the density must be considered. All glass samples are shown to have high density values ranging from 4.914 – 4.934 gcm^{-3}. Figure 1 shows the variation of density and molar volume of the synthesized glasses with concentration of CuO NPs. It is evident that the density increases nonlinearly with increase in CuO NPs content, while molar volume decreases nonlinearly with CuO NPs content. The increase of CuO NPs concentration caused an increase of non-bridge oxygen (NBO) ratio in network, and led to a compact structure [24]. It is generally expected that density and molar volume sare inversely related to each other and the same is reported in the present investigated glasses. This behaviour also reported by previous [25]. Addition of CuO NPs decreased the molar volume related to the reduction of total volume [26]. Decrease in molar volume signified the reduction of interatomic spacing in the network [27]. The incorporation of CuO NPs into the glass network increased the hardness of the glass from 262 – 349 GPa. The decreases of free volume by addition of CuO NPs provide fewer voids in the glass, hence improved the compactness of the prepared glass [28]. The refractive index, molar refractivity and polarizability were enhanced from 2.42 – 2.763, 16.775 – 18.298 cm^3/mol and 6.649 – 7.253×10^{-24} cm^3 respectively. Glasses with lower band gap energy become more compact and have high refractive index [29]. The formations of TeO_3 and TeO_{3+1} create more NBO, thus reorganized the network structure of the tellurite glass and leads to the increased in the polarizability. The NBOs has higher polarizability than BOs and make the glass become polarized [28]. Larger ionic radius of Cu^{2+} (0.73Å) than Te^{4+} (0.66 Å) affect the refractive index. Besides, Cu^{2+} (3.75 Å) have lower field strength (field strength = Z/r^2 where Z and r is oxidation number and ionic radius respectively) than Te^{4+} (9.18 Å). Thus, Cu^{2+} ions are easily to polarized [24].

The variations of ionic packing density in the proposed glass samples are enlisted in Table 2. The ionic packaging density slightly increases with the increment of CuO NPs contents up to 0.1 mol% and reduced at 0.25 mol%. Reduction of V_t could be describe using atomic radius of

an atom. Cu^{2+} (0.73 Å) have larger ionic radius that Te^{4+} (0.66 Å) and higher tendency to fit the excess volume. Thus, the glass compactness decreased. Furthermore, increase in molar volume lead to the reduction of V_t. Split behavior the value turn back to increase with addition of CuO NPs above 0.25 mol% due to the CuO NPs completely filled the space of excess volume. Thus, the glass becomes more compact.

Table 2. *Various physical and optical properties of glasses with different concentrations of CuO NPs.*

Properties	Glass Sample					
	S1	S2	S3	S4	S5	S6
Physical Properties						
Density, ρ (g cm^{-3})	4.914	4.916	4.905	4.926	4.930	4.934
Molar volume, V_M (cm^3 mol^{-1})	26.919	26.899	26.935	26.782	26.677	26.575
Hardness (GPa)	262	272	324	345	349	337
Refractive index, n	2.442	2.498	2.537	2.595	2.654	2.763
Molar refractivity, R_M (cm^3/ mol)	16.775	17.108	17.355	17.582	17.829	18.298
Polarizability, α_e ($\times 10^{-24}$ cm^3)	6.649	6.781	6.879	6.969	7.067	7.253
Ionic packaging density, V_t	0.464	0.465	0.463	0.466	0.466	0.467
Optical properties						
Energy band gap, E_g (eV)	2.85	2.64	2.53	2.36	2.20	1.94
Urbach energy, E_u (eV)	0.12	0.14	0.16	0.17	0.18	0.19

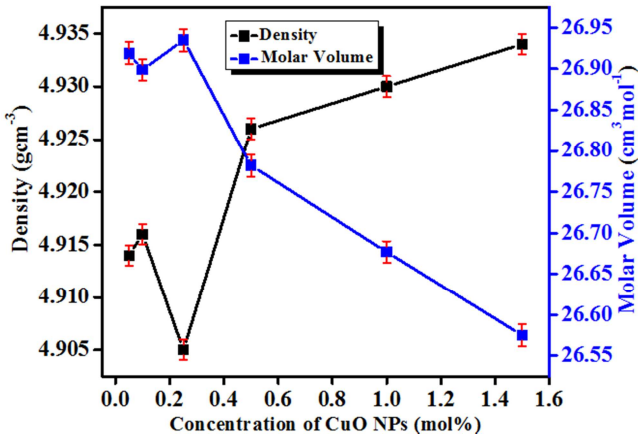

Figure 1. *Variation of density and molar volume with different concentration of CuO NPs in the prepared glass system.*

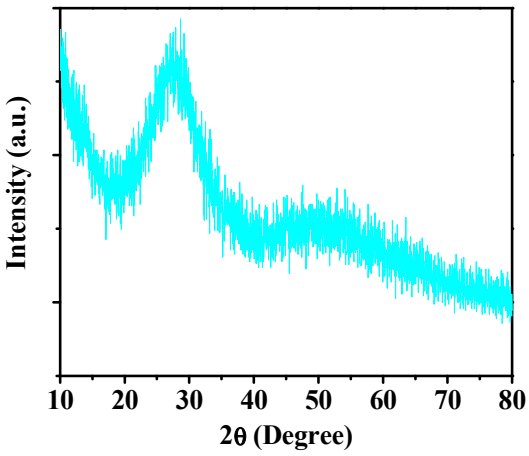

Figure 2. *CuO NPs concentration (mol%) dependent XRD patterns of S5 glass sample.*

3.2. XRD and HRTEM

Figure 2 shows the XRD patterns of the prepared S5 glass sample containing 1.0 mol% CuO NPs. That presence of a broad hump at about 15-35° indicates the non-crystallinity of this sample, and absence of any crystalline phase. In general, a glass is supposed to be a random arrangement of molecules and below the transformation region; the molecules are much less mobile. The diffraction lines of metallic CuO particles are not observable due to either small concentration of CuO NPs in the crystalline phase, and/or large scattering and absorption of heavy metal tellurite oxide, which probably annihilate any other weaker signal. Although the diffraction patterns of metallic NPs are rarely observed in some oxide glasses, in general, the absence of latter lines in XRD profile could not credit the lack of NPs formed within this matrix. In order to confirm the formation of CuO NPs in these tellurite glasses, HRTEM imaging technique is employed.

Figure 3 shows HRTEM images of 1.0 mol% CuO NP (S5). By analyzing the HR-TEM image, the average distance between the crystal planes is estimated for the crystalline metal species. The presence of crystalline CuO NPs was confirmed by the measurement of lattice spacing with 0.23 nm attributed well to the spacing between (111) plane of CuO NPs as shown in Figure 3(a). This result matched with the JCPDS card No. 00-001-1117. The presence of CuO NPs is in the glass matrix has face centred cubic symmetry which is proven by Fast Fourier Transformation (FFT) as shown in Figure 3(b).

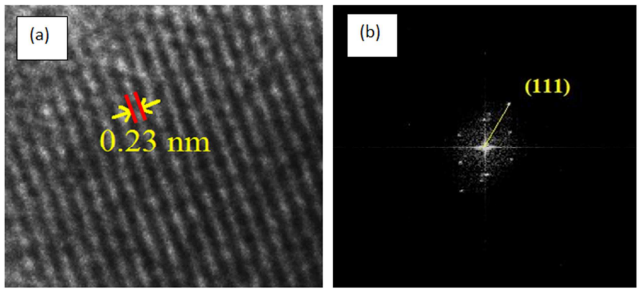

Figure 3. *(a) HRTEM image of CuO NPs (b) corresponding FFT image.*

3.3. FTIR

Figure 4 displays the IR transmissions spectra for all glass samples. The band assignments are shown in Table 3. The

present results displays are in the same manner with previous studies. Five significance bands are observed. Hence the IR absorption spectra are as follows. The observed IR band at 453 – 460 cm^{-1} is assigned to the Te-O-Te linkages where bending vibration happened while the band located at 588 – 602 cm^{-1} can be ascribed to the TeO_4 stretching vibrations with BO [30]. Breakdown of Te-O-Te linkages from TeO_4 unit into TeO_3 unit with the embedment of CuO NPs change the structure of the glass along with the addition of NBO [32]. The observed bands at 708 – 722 cm^{-1} are due to the TeO_3 bending vibration with NBO [31]. The non-existence of tellurite oxide, TeO_2 assignment in FTIR spectra shows that the bridging oxygen of tellurite oxide, TeO_2 is completely converted to non-bridging oxygen. Moreover, the bands at 1627 – 1641 cm^{-1} corresponds to the M-OH bending vibration. Further addition of CuO NPs causing the absorption peaks intensity of OH stretching vibration become smaller at 3472 – 3494 cm^{-1}. The smaller the difference in electronegativity between ions, the weaker the absorption peaks [32].

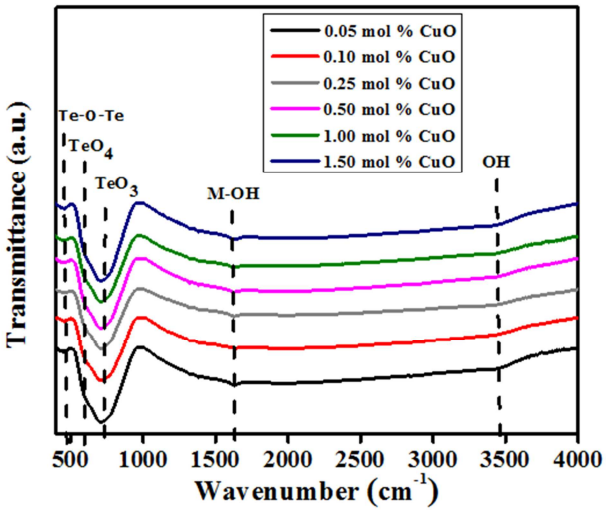

Figure 4. *FTIR spectra as a function of varying CuO NPs concentrations.*

Table 3. *Band assignment of glass with silver nanoparticles.*

Sample	CuO (mol%)	FTIR Shift (cm^{-1})				
		Te-O-Te (Bending vibration)	TeO_4 (Stretching vibration)	TeO_3 (Bending vibration)	M-OH (Bending vibration)	OH (Stretching vibration)
S1	0.05	453	609	708	1627	3472
S2	0.10	453	602	722	1641	3494
S3	0.25	460	602	722	1641	3494
S4	0.50	460	602	715	1639	3479
S5	1.00	460	602	715	1641	3472
S6	1.50	460	615	715	1641	3479

3.4. Optical Absorption Spectra

The optical absorption spectra of Er^{3+} doped tellurite glass with CuO NPs are presented in Figure 5. It can be seen the absorption spectra consist of seven transitions that are observed from the ground sate $^4I_{15/2}$ to the excited states $^4F_{7/2}$, $^2H_{11/2}$, $^4S_{3/2}$, $^4F_{9/2}$, $^4I_{9/2}$, $^4I_{11/2}$ and $^4I_{13/2}$ are attributed to excited states around 488, 522, 545, 652, 799, 973 and 1530 nm. The increment of CuO NPs enhanced the absorption of the glass and resulting the appearance of broad absorption peak due to the characteristic of CuO NPs. Electronic transition of Cu^{2+} occur around the near infrared (NIR) region at more than 600 nm [33]. The presence of broad peak corresponds to the spin allowed transition from $^2E_g \rightarrow {}^2T_{2g}$ energy levels in octahedral symmetry of divalent Cu^{2+} ions in these glasses [30]. Three wider peak are expected to presence attributed to $^2B_{Ig} \rightarrow {}^2A_{1g}$, $^2B_{Ig} \rightarrow {}^2B_{2g}$ and $^2B_{Ig} \rightarrow {}^2E_g$ transitions. The broad peak of Cu^{2+} are due to the overlapping of the three transition overlapped forming single band and are in agreement with the other finding [34].

Absorption spectra are used to determine the optical band gap in the glass samples. The study of optical band is significant for predicting the wavelength of light that will be absorbed by the sample material. Energy band gap, E_g are obtained from extrapolating the straight line of plots of $(\alpha h\upsilon)^{1/2}$ versus photon energy ($h\upsilon$) at $(\alpha h\upsilon)^{1/2} = 0$. Urbach energy, E_u can be determine from the inverse of the calculated gradient, 1/m that are obtained from the slope of absorption coefficient ln (α(υ)) versus photon energy ($h\upsilon$). The strong dependence of E_g with the increase of CuO NPs content is shown in Figure 6. The decrease in energy band gap is attributed to the decrease in average bond energy. Increase of more NBOs than BOs in the glass system lowering the average bond and leads to the decreasing of E_g. Larger number of NBO produce more negatively charged ions signifies more of localized electrons in the glass network and allowed the electron to easily jump from valence band to conduction band [28].

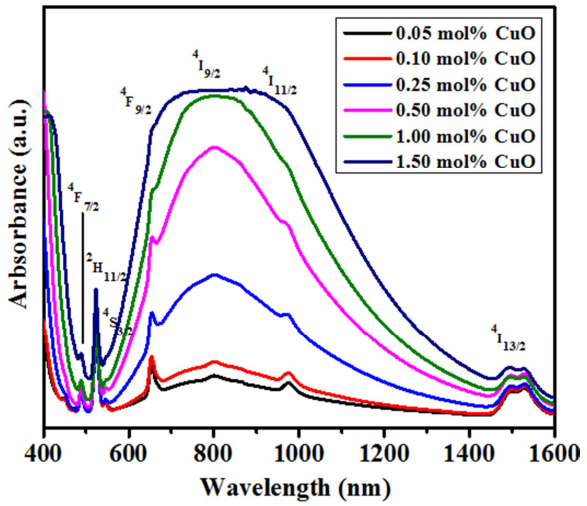

Figure 5. *Absorption spectrum of studied glass.*

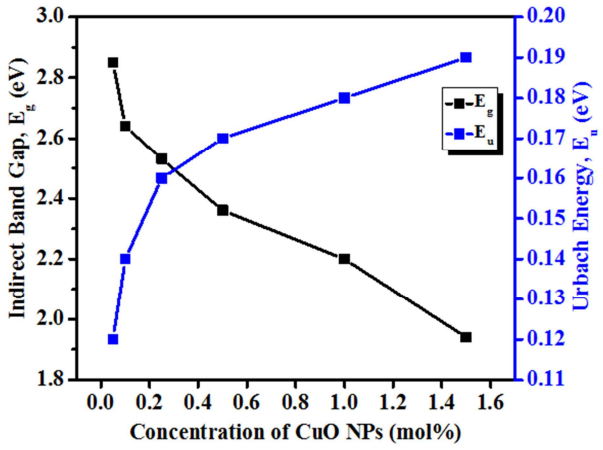

Figure 6. *The dependence of E_g and E_u of studied glass.*

Generally, the band tailing (a measure of the defect states or materials disorder) in the forbidden optical energy band gap that exists in the glass and amorphous materials are characterized in terms of the Urbach energy. High value of the E_u indicated the strong disorder of the glass due to the extension of the localized states within the band gap where the glass have larger tendency to transform the weak bonds into defects. In contrast, the minimum E_u indicated less disorder and compactness. The E_u of the studied glass was found to increase with increasing CuO NPs concentrations. This indicates the disorder in the glass increase as a result of high number of extension of the localized states between gaps [27].

The nephelauxetic effect is known as the expansion of electron cloud which is caused by the overlapping of the metal and ligand orbitals. The bonding parameter (δ) is related to the nature of the RE-O bond where the positive value depicts the covalent nature while negative value shows the ionic nature. Table 4 summarized the average nephelauxetic ratio and bonding parameter of the prepared glass samples. The bonding parameter exhibits negative sign indicates the bonding in the prepared tellurite glass network is ionic bonding between the Er^{3+} ion and the ligands. where the ionic nature gradually decrease with the addition CuO NPs. Increasing of CuO NPs contents lead to the rise of covalent character resulting from the upward shift in δ values. Conversely, the calculated value of nephelauxetic ratio present opposite trend with the addition of CuO NPs. This result is in agreement with the previous finding [35]. The β values decreased due to the decreasing effective positive charge of Er^{3+} ions by attracting electron from ligands resulting expansion of *d*-orbital of Er^{3+} ions. Larger electron cloud formed and overlapping between *d*-orbital of Er^{3+} ions and ligand orbital leads to the reduction of interelectronic repulsion between Er^{3+} ions and ligand, thus increases the covalent bonds [36]. Therefore, the lower the values of β, the greater the formation of electron cloud, the higher the value of δ and brings to the enhancement of the covalent bond between Er^{3+} and the surrounding ligand [1].

Table 4. *Nephelauxetic ratio and bonding parameter of Er^{3+} doped tellurite glass with CuO NPs embedment at different absorption transition.*

Characteristic Transition (cm^{-1})	CuO NPs Concentration (mol%)						
	0.05	0.10	0.25	0.50	1.00	1.50	Aquo [28]
$^4F_{7/2} \rightarrow {}^4I_{15/2}$	20491	20491	20449	20449	20491	20491	20450
$^2H_{11/2} \rightarrow {}^4I_{15/2}$	19157	19157	19157	19157	19157	19157	19150
$^4S_{3/2} \rightarrow {}^4I_{15/2}$	18348	18348	18348	18348	18348	18348	18350
$^4F_{9/2} \rightarrow {}^4I_{15/2}$	15313	15313	15313	15313	15313	15313	15250
$^4I_{9/2} \rightarrow {}^4I_{15/2}$	12500	12500	12500	12484	12453	12453	12400
$^4I_{11/2} \rightarrow {}^4I_{15/2}$	10266	10266	10256	10245	10235	10235	10250
$^4I_{13/2} \rightarrow {}^4I_{15/2}$	6622	6618	6613	6618	6613	6609	6600
$\bar{\beta}$	1.0024	1.0024	1.0018	1.0016	1.0016	1.0015	1
Δ	-0.241	-0.237	-0.181	-0.160	-0.156	-0.152	0

3.5. Optical Emission Spectra

Figure 7 represents down-conversion (DC) luminescence spectra of Er^{3+} ion under excitations 380 nm. Four distinctive emission spectra centered at 408, 530, 550 and 660 nm allocated respectively to $^4F_{3/2} \rightarrow {}^4I_{15/2}$, $^2H_{11/2} \rightarrow {}^4I_{15/2}$, $^4S_{3/2} \rightarrow {}^4I_{15/2}$ and $^4F_{9/2} \rightarrow {}^4I_{15/2}$ transitions. Obviously, the intensity of green band at 550 nm is higher than green bands at 530 nm and with other blue and red bands. It can be observed that as the intensity of CuO NPs content increased, the intensity of emission spectra decreased. This result is similar with the result obtained by J. A. Jimenez in copper–samarium–aluminophosphate glasses due to the energy transfer between excited state of $Er^{3+} \rightarrow Cu^{2+}$ that act as reverse process from enhancement in PL intensity [21]. Besides, the quenching effect is responsible from the large formation of multipoles interaction that leads to the energy transfer from RE ions to NPs [25].

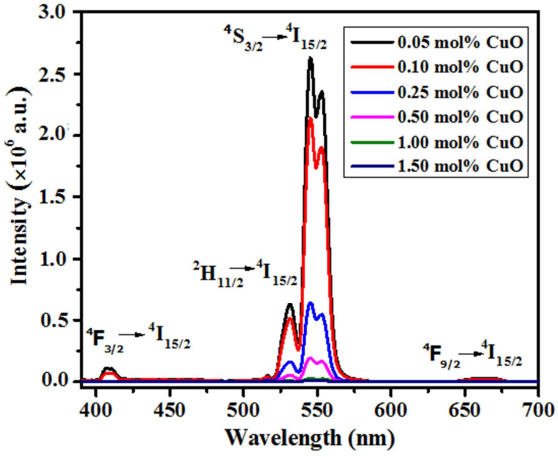

Figure 7. *Down-conversion photoluminescence spectra with different concentrations of CuO NPs.*

Figure 8 shows the characteristic Up-conversion (UC) emission spectra for all samples upon 980 nm excitations. The PL spectra exhibits three emissions peaks centered at 530, 550 and 660 nm attributed to the indicated emission transitions $^2H_{11/2} \rightarrow {}^4I_{15/2}$, $^4S_{3/2} \rightarrow {}^4I_{15/2}$ and $^4F_{9/2} \rightarrow {}^4I_{15/2}$, respectively. It is found that, further addition of CuO NPs causing the emissions to diminish. The luminescence quenching due to the energy transfer (thermal energy dissipation) from the excited Er^{3+} ions to the CuO NPs [28]. Furthermore, CuO NPs has electronic configuration of [Ar]$3d^9$ which has one unpaired electron. Thus, CuO NPs considered as para magnetism [38]. The energy transfer due to nucleation and large amount of NPs aggregates around Er^{3+} ions causing overlapping of electric field. As a result, local field effect mediated energy transfer from CuO NPs to Er^{3+} decreased. The transfer of energy due to the transformation of singlet to triplet states [36]. Previous study reported, an EPR signal are detected using Electron Paramagnetic Resonance (EPR) spectroscopy for all samples that indicates the paramagnetic behaviour of Cu^{2+} ions [19]. This result also in agreement with the result obtained by S. Suresh *et al.* that display same spectral behavior [30].

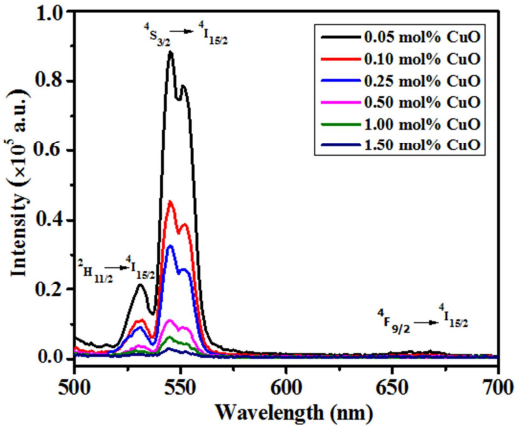

Figure 8. *Up-conversion photoluminescence spectra with different concentrations of CuO NPs.*

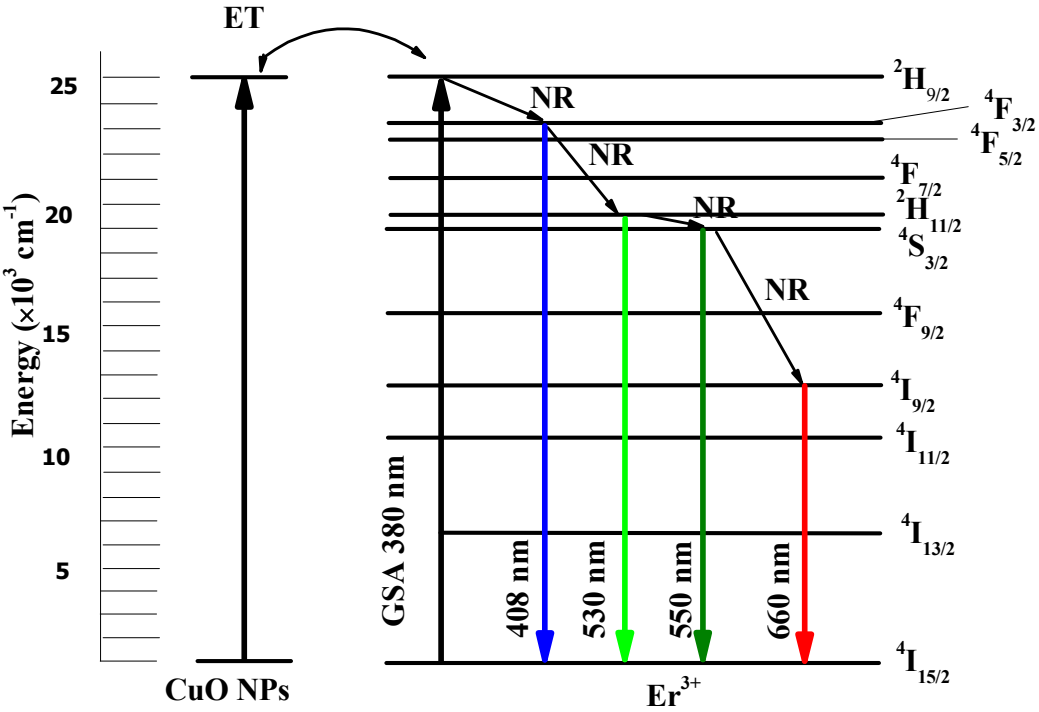

Figure 9. *Partial energy level diagram for Er^{3+} ions in tellurite glass for down-conversion with CuO NPs in the vicinity.*

Partial energy level diagram of Er^{3+} ions incorporated with CuO NPs are schematically illustrated in Figure 9 and Figure 10 to describe the mechanisms involved in the emission process. Figure 9 displays energy transfer of down-conversion emissions spectra through ground state absorption (GSA), energy transfer (ET) and non-radiative decay (NR) processes. Upon laser excitation, the ions from the ground state, $^4I_{15/2}$ are excited to the $^2H_{9/2}$ energy level via GSA. Then, NR decays populate to the lower excited states $^4F_{3/2}$, ($^2H_{11/2}$, $^4S_{3/2}$) and $^4I_{9/2}$ levels and the energy loss disappeared in form of heat throughout this process [39]. Then, radiative decay from $^4F_{3/2} \rightarrow {}^4I_{15/2}$ responsible for the blue emission located at 408 nm. The green emissions at 530 and 550 nm originate from the transitions $^2H_{11/2} \rightarrow {}^4I_{15/2}$ and $^4S_{3/2} \rightarrow {}^4I_{15/2}$, respectively. The transition from $^4F_{9/2} \rightarrow {}^4I_{15/2}$ attributed to the red emission at 660 nm. However, luminescence quenching is obtained due to the ET from Er^{3+} ions to CuO NPs. The transfer of energy due to the high number of clustering of CuO NPs around Er^{3+} ions resulting overlapping of the electric field [36]. The energy transfer producing more energy into heat [37]. Figure 10 shows the up-conversion emission spectra at 530, 550, and 660 nm. The first incident photon of 980 nm excitation wavelengths is stimulated and absorbed by Er^{3+} ions. Then, the Er^{3+} ions are promoted to

$^4I_{11/2}$ ($^4I_{15/2} \rightarrow {}^4I_{11/2}$) energy level. In ESA process, Er^{3+} ions absorb photons and excited to higher excited states $^4F_{7/2}$ ($^4I_{11/2} \rightarrow {}^4F_{7/2}$) [22]. The NR decay from $^4F_{7/2}$ to $^2H_{11/2}$ and from $^2H_{11/2}$ to $^4S_{3/2}$ populates these level and leads to the green emission. The other transition via $^4S_{3/2}$ to $^4I_{9/2}$ brings to the red emissions.

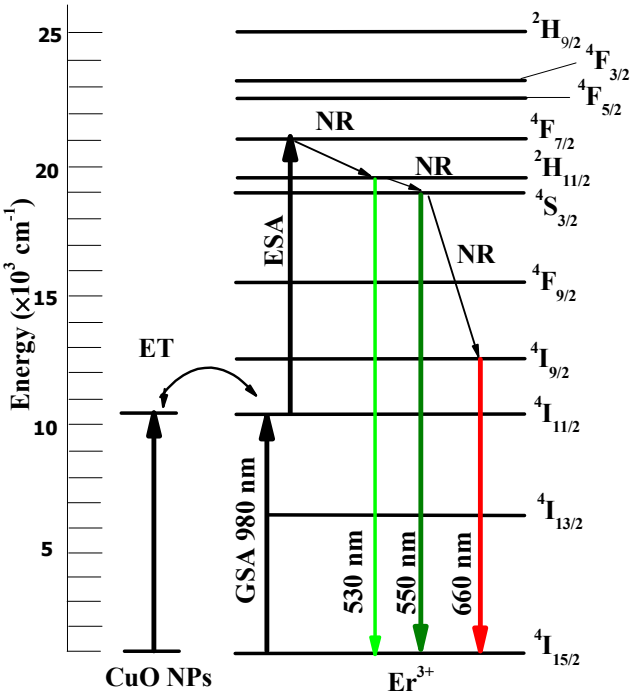

Figure 10. *Partial energy level diagram for Er^{3+} ions in tellurite glass for up-conversion with CuO NPs in the vicinity.*

4. Conclusions

The present investigation was interested in preparing the Er^{3+} doped tellurite glass with CuO NPs embedment, which has been prepared by melt quenching technique. The incorporation of CuO NPs changes the structure of the glass with the addition of more NBOs. The variations of physical properties with the addition of CuO NPs signify the glass becomes more compact. The presence of crystalline CuO NPs in the glass network is confirmed using HRTEM image. The absorption spectrum reveals seven prominent peaks that enhanced with the addition of CuO NPs. The disorder in the glass increased with the decrease of energy band gap and increase in Urbach energy. The intensity quenching in both down- and upconversion spectra is attributed to the energy transfer from Er^{3+} ions to CuO NPs. Furthermore, the intense of green band PL emission may be contributed as a promising material toward the development of laser and photonic devices.

5. Recommendation for Further Study

Analytical techniques such as XRD, FTIR, HRTEM, UV-Vis absorption and PL emission spectroscopy have been used and showed that structural and optical characteristics of proposed glass system has improved by addition of Cu NPs. However, there are many characteristic analysis which are not provided yet due to some limitations. The prepared glass can further be investigated through Raman spectroscopy, Nuclear-Magnetic Resonance (NMR), and Electron-Spin Resonance (ESR). Studied glass may be examined by addition of other dopants in order to increase the absorption and emission cross-sections of Er^{3+} ions.

Acknowledgements

The authors gratefully acknowledge the financial support from Ministry of Education, Malaysia and Universiti Teknologi Malaysia via grants of Vot: 02K41, 4B329, 05H45, 05H36, 4F424, 4F319, 4F083, and 07J80.

References

[1] Yusoff, N. M., Sahar, M. R. (2015). The incorporation of Silver Nanoparticles in Samarium doped Magnesium Tellurite Glass: Effect on the Characteristic of Bonding and Local Structure. *Phys. B Condens. Matter*, 470–471: 6–14.

[2] Yousef, E. S., Elokr, M. M., Aboudeif, Y. M. (2016). Optical, Elastic Properties and DTA of TNZP Host Tellurite Glasses doped with Er^{3+} Ions. *J. Mol. Struct.*, 1108: 257–262.

[3] Sazali, E. S., Sahar, M. R., Ghoshal, S. K., Arifin, R. (2014). Optical Properties of Gold Nanoparticle Embedded Er^{3+} Doped Lead–Tellurite Glasses. *J. Alloys Compd,* 607: 85–90.

[4] Azlan, M. N., Halimah, M. K., Sidek, H. A. A. (2017). Linear and Nonlinear Optical Properties of Erbium doped Zinc Borotellurite Glass System. *J. Lumin,* 181: 400–406.

[5] Mahraz, Z. A. S., Sazali, E. S., M. R., Sahar, Amran, N. U., Yaacob, S. N. S., Aziz, S. M., Mawlud, S. Q., Noor, F. M., Harun, A. N. (2019). Spectroscopic Investigations of Near-infrared Emission from Nd^{3+}-Doped Zinc-Phosphate Glasses: Judd-Ofelt Evaluation, *J. Non. Cryst. Solids*, 509: 106–114.

[6] Nawaz, F., Sahar, M. R., Ghoshal, S. K., Amjad, R. J., Dousti, M. R., Awang, A. (2013). Spectral Investigation of Sm^{3+}/Yb^{3+} Co-doped Sodium Tellurite Glass. *Chinese Opt. Lett*, 11: 061605-4.

[7] Reza Dousti, M., Junaid Amjad, R. (2017). Effect of Silver Nanoparticles on the Upconversion and Near-infrared Emissions of Er^{3+}:Yb^{3+} Co-doped Zinc Tellurite Glasses. *Measurement,* 105: 114-119.

[8] Kaiyu, T., Yumian, Y., Huizhong, B., Shuangbao, W. (2021). Synthesis and Luminescence Characteristics of Tb^{3+}-Doped Fluorophosphate Glass for UV Detection. *J. Non. Cryst. Solids,* 572: 121012.

[9] Wantana, N., Kaewnuam, E., Ruangtaweep, Y., Valiev, D., Stepanov, S., Yamanoi, K., Kim, H. J., Kothan, S., Kaewkhao, J. (2021). Tunable Orange, Yellow and White Emission of Pr^{3+}-Doped Tungsten Gadolinium Borate Glasses. *J. Non. Cryst. Solids,* 554: 120630.

[10] Hasim, N. B. (2017). *Effects of Embedded Silver Nanoparticles on Physicals and Optical Properties of Erbium and Neodymium Codoped Lithium Niobate Tellurite Glass.* University Teknologi Malaysia.

[11] Danmallam, I. M., Ghoshal, S. K., Ariffin, R., Jupri, S. A., Sharma, S. (2019). Europium Ions and Silver Nanoparticles Co-doped Magnesium-Zinc-Sulfophosphate Glasses: Evaluation of Ligand Field and Judd-Ofelt Parameters. *J. Lumin*. 216: 116713.

[12] Ashok, J., Kostrzewa, M., Ingram, A., Venkatramaiah, N., Srinivasa Reddy, M., Ravi Kumar, V., Piasecki, M., Veeraiah, N. (2019). Structural and Dielectric Features of Silver Doped Sodium Antimonate Glass Ceramics. *J. Alloys Compd*, 791: 278–295.

[13] Awang, A., Ghoshal, S. K., Sahar, M. R., Arifin, R., Nawaz, F. (2014). Non-spherical Gold Nanoparticles Mediated Surface Plasmon Resonance in Er^{3+} Doped Zinc-Sodium Tellurite Glasses: Role of Heat Treatment. *J. Lumin*, 149: 138–143.

[14] Dousti, M. R., Amjad, R. J., Mahraz, Z. A. S. (2015). Enhanced Green and Red Upconversion Emissions in Er^{3+}-Doped Boro-Tellurite Glass Containing Gold Nanoparticles. *J. Mol. Struct*, 1079: 347-352.

[15] Jimenez, J. A. (2013). Effect Influence of Ag Nanoparticles on the Luminescence Dynamics of Dy^{3+} Ions in Glass: the ''Plasmonic Diluent''. *Phys. Chem. Chem. Phys*, 15: 17587-17594.

[16] Amjad, R. J., Dousti, M. R., Iqbal, A., Hussain, S. Z., Sahar, M. R., Shaukat, S. F. (2015). Influence of Silver Nanoparticles on the Luminescence Dynamics of Dy^{3+} Doped Amorphous Matrix. *Measurement*, 74: 87-9.

[17] Chiasera, A., Ferrari, M., Mattarelli, M., Montagna, M., Pelli, S., Portales, H., Zheng, J., Righini, G. C. (2005). Assessment of Spectroscopic Properties of Erbium Ions in a Soda-Lime Silicate Glass After Silver–Sodium Exchange. *Opt. Mater*, 27: 1743-1747.

[18] Dousti, M. R., Poirier, G. Y., Amjad, R. J., de Camargo, A. S. S. (2016). Luminescence Quenching Versus Enhancement in WO_3-$NaPO_3$ Glasses Doped With Trivalent Rare Earth Ions and Containing Silver Nanoparticles. *Opt. Mater*, 60: 331-340.

[19] Bhogi, A., Vijaya K. R., Kistaiah, P. (2015). Effect of Alkaline Earths on Spectroscopic and Structural Properties of Cu^{2+} Ions–doped Lithium Borate Glasses. *J. Non. Cryst. Solids,* 426: 47–54.

[20] Barna, S. F., Ramanathan, A., Jacobs, K. E., Mensing, G. (2017). Solid State Electrochemical Direct Writing of Copper Nanostructures on an Ion Conductive Phosphate Glass Using Atomic Force Microscopy. *Procedia Manuf,* 10: 641–651.

[21] Jiménez, J. A. (2015). Samarium (III) as luminescent probe for copper (II). *J. Lumin,* 161: 352–357.

[22] Mahraz, Z. A. S., Sahar, M. R., Ghoshal, S. K. (2017). Reduction of Non-Radiative Decay Rates in Boro-Tellurite Glass via Silver Nanoparticles Assisted Surface Plasmon Impingement: Judd Ofelt Analysis. *J. Lumin,* 190: 335–343.

[23] Awang, A., Ghoshal, S. K., Sahar, M. R., Arifin, R. (2015). Gold Nanoparticles Assisted Structural and Spectroscopic Modification in Er^{3+}–doped Zinc Sodium Tellurite Glass. *Opt. Mater. (Amst),* 42: 495–505.

[24] Yusoff, N. M., Sahar, M. R. (2015). Effect of Silver Nanoparticles Incorporated with Samarium-doped Magnesium Tellurite Glasses. *Phys. B Condens. Matter,* 456: 191–196.

[25] Dousti, R. M., Sahar, M. R., Ghoshal, S. K., Amjad, R. J., Samavati, A. R. (2013). Effect of AgCl on Spectroscopic Properties of Erbium doped Zinc Tellurite Glass. *J. Mol. Struct,* 1035: 6–12.

[26] Sazali, E. S., Sahar, M. R., Ghoshal, S. K., Arifin, R. (2015). Efficient Optical Enhancement of Er^{3+} doped Lead-Tellurite Glass Embedded with Gold Nanoparticles: Role of Heat-Treatment. *J. Non. Cryst. Solids*, 410: 174–179.

[27] Awang, A., Ghoshal, S. K., Sahar, M. R., Dousti, R. M. (2013). Enhanced Spectroscopic Properties and Judd-Ofelt Parameters of Er-doped Tellurite Glass: Effect of Gold Nanoparticles. *Curr. Appl. Phys,* 13: 1813–1818.

[28] Yusof, N. N., Ghoshal, S. K., Ari, R., Awang, A. (2018). Self-Cleaning and Spectral Attributes of Erbium doped Sodium-Zinc-Tellurite Glass : Role of Titania Nanoparticles. *J. Non. Cryst. Solids*, 481: 225–238.

[29] Widanarto, W., Sahar, M. R., Ghoshal, S. K., Arifin, R. (2013). Natural Fe_3O_4 Nanoparticles Embedded Zinc-Tellurite Glasses: Polarizability and Optical Properties. *Mater. Chem. Phys,* 138: 174–178.

[30] Suresh, S., Pavani, P. G., Mouli, V. C. (2012). ESR, Optical Absorption, IR and Raman Studies of $xTeO_2$+(70-x)B_2O_3+5TiO_2+24R_2O:1CuO (x=10, 35 and 60 mol%; R = Li, Na and K) Quaternary Glass System. *Mater. Res. Bull,* 47: 724–731.

[31] Tanko, Y. A., Ghoshal, S. K., Sahar, M. R. (2016). Ligand Field and Judd-Ofelt Intensity Parameters of Samarium doped Tellurite Glass. *J. Mol. Struct,* 1117: 64–68.

[32] Amjad, R. J., Dousti, M. R., Sahar, M. R. (2015). Spectroscopic Investigation and Judd-Ofelt Analysis of Silver Nanoparticles Embedded Er^{3+}-doped Tellurite Glass. *Curr. Appl. Phys,* 15: 1–7.

[33] Richardson, H. W. (1997). *Handbook of Copper Compounds and Applications,* Marcel Dekker Inc.

[34] Gaafar, M. S., Marzouk, S. Y. (2017). Judd–Ofelt Analysis of Spectroscopic Properties of Er^{3+} doped TeO_2–BaO–ZnO Glasses. *J. Alloys Compd,* 723: 1070–1078.

[35] Dousti, R. M., Ghassemi, P., Sahar, M. R., Mahraz, Z. A. (2014). Chemical durability and Thermal Stability of Er^{3+}-doped Zinc Tellurite Glass Containing Silver Nanoparticles. *Chalcogenide Lett,* 11: 111–119.

[36] Aziz, S. M., Sahar, M. R., Ghoshal, S. K. (2018). Spectral Attributes of Eu^{3+} doped Borotellurite Glasses Containing Mn_3O_4 Nanoparticles. *J. Alloys Compd,* 735: 1119–1130.

[37] Yusof, N. N., Ghoshal, S. K., Azlan, M. N. (2017). Optical Properties of Titania Nanoparticles Embedded Er^{3+}-doped Tellurite Glass: Judd-Ofelt analysis. *J. Alloys Compd,* 724: 1083–1092.

[38] Reddy, S. L., Endo, T., Reddy, G. S.(2012). Electronic (Absorption) Spectra of 3d Transition Metal Complexes. 3–48.23234.

[39] Aziz, S. M., Sahar, M. R., Ghoshal, S. K. (2017). Modified Magnetic and Optical Properties of Manganese Nanoparticles Incorporated Europium doped Magnesium Borotellurite Glass. *J. Magn. Magn. Mater,* 423: 98–105.